

Exploring Techniques for the Analysis of Spontaneous Asynchronicity in MPI-Parallel Applications

Ayesha Afzal¹, Georg Hager¹, Gerhard Wellein^{1,2}, and Stefano Markidis³

¹ Erlangen National High Performance Computing Center (NHR@FAU), 91058 Erlangen, Germany,

² Department of Computer Science, University of Erlangen-Nürnberg, 91058 Erlangen, Germany,

³ Department of Computer Science, KTH Royal Institute of Technology, 11428 Stockholm, Sweden, ayesha.afzal@fau.de, georg.hager@fau.de, gerhard.wellein@fau.de, markidis@kth.se

Abstract. This paper studies the utility of using data analytics and machine learning techniques for identifying, classifying, and characterizing the dynamics of large-scale parallel (MPI) programs. To this end, we run microbenchmarks and realistic proxy applications with the regular compute-communicate structure on two different supercomputing platforms and choose the per-process performance and MPI time per time step as relevant observables. Using principal component analysis, clustering techniques, correlation functions, and a new “phase space plot,” we show how desynchronization patterns (or lack thereof) can be readily identified from a data set that is much smaller than a full MPI trace. Our methods also lead the way towards a more general classification of parallel program dynamics.

1 Introduction and related work

Highly parallel MPI programs with no or weak global synchronization points show interesting dynamics that go beyond what is expected from their usually regular compute-communicate structure. Initiated by what is typically called “noise,” a plethora of patterns can emerge: Propagating delays emanating from strong one-off disturbances, so-called *idle waves* [9], can interact [3] and eventually decay [1, 2, 3] via various mechanisms. Caused by idle waves, but also under the natural, fine-grained system noise, some applications are unstable and leave their initial lock-step mode (Figure 2 (left)) where all processes either compute or communicate. It was shown [2] that a hardware bottleneck such as main memory bandwidth is a prerequisite for this *bottleneck evasion* to occur. As a consequence, such programs settle in a metastable state, a *computational wavefront*, where neighboring processes are shifted in time with respect to each other (Figure 2 (right)). It was also shown [4] that this *desynchronization* can lead to substantial speedups via automatic overlap of communication and code execution.

Investigating these dynamics typically requires the analysis of MPI traces taken by tools such as Intel Trace Analyzer/Collector or VAMPIR. Apart from the often prohibitive amount of data contained in such traces, the relevant patterns are often hidden in the data and not readily visible to the human eye. Furthermore, it is hard, if not impossible, to obtain this data in a production environment without adverse effects on the performance of applications. For applications that have natural regular compute-communicate cycles, we propose to use the MPI waiting time per process and time step (i.e., the time spent in the MPI library, regardless of whether communication takes place or not) as a starting point and input metric for data analysis methods that can identify the structural processes described above. The performance per process and time step can serve as a supplemental metric to track the impact of automatic communication overlap.

This paper makes the following relevant contributions:

Table 1: Key hardware and software properties of systems.

| Systems | Meggie | Fritz |
|------------------------------|-------------------------|-----------------------------------|
| Processor | Intel Xeon Broadwell EP | Intel Xeon Ice Lake |
| Processor Model | E5-2630 v4 | Platinum 8360Y |
| Base clock speed | 2.2 GHz | 2.4 GHz |
| Physical cores per node | 20 | 72 |
| Numa domains per node | 2 | 2 |
| Last-level cache (LLC) size | 25 MB (L3) | 54 MB (L3) |
| Memory per node (type) | 64 GB (DDR4) | 256 GB (DDR4) |
| Theor. memory bandwidth | 68.3 GB/s | 102.4 GB/s |
| Node interconnect | Omni-Path | Infiniband |
| Interconnect topology | Fat-tree | Fat-tree |
| Raw bandwidth p. link n. dir | 100 Gbits ⁻¹ | 100 Gbits ⁻¹ |
| Compiler | Intel C++ v2019.5.281 | intel C++ v2021.4.0 |
| Message passing library | Intel MPI v2019u5 | intelmpi/2021.4.0 |
| Operating system | CentOS Linux v7.7.1908 | AlmaLinux v8.5 rhel centos fedora |

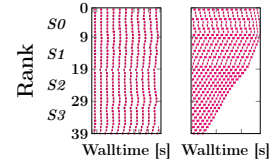
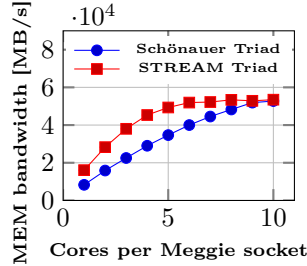


Fig. 2: Timeline traces of synchronized (left) and desynchronized (right) MPI processes on sockets (S_i).

Fig. 1: Saturation attributes

- We demonstrate how to automatically characterize different flavors of synchronous versus non-synchronous execution of MPI-parallel codes without taking full MPI traces or in-depth application analysis.
- We show that the MPI waiting time per process and time step provides a powerful input metric for principal component analysis (PCA) and clustering methods in order to spot these patterns.
- We introduce the *MPI phase space plot* as a tool to visualize the long-term evolution and peculiar patterns of MPI waiting time in a parallel program.

This paper is organized as follows: We first provide details about our experimental environment and methodology in Sect. 2. To investigate the dynamics of large-scale parallel programs, simple metrics such as the histogram and timelines for all or individual MPI processes are studied in Sect. 3, while Sect. 4 covers advanced methods like correlation coefficient matrices and phase space plots. Sect. 5 addresses machine learning techniques such as Principal Component analysis and k-means clustering. Finally, Sect. 6 concludes the paper and gives an outlook to future work.

2 Case studies, testbed and experimental methods

2.1 Test systems and methodology

The details of the hardware and software environments on the “Meggie”⁴ and “Fritz”⁵ clusters can be found in Table 1. By default, hyper-threading (SMT) is disabled on both systems and Sub-NUMA Clustering (SNC) is enabled on the Fritz system. The optimization flag `-O3` was utilized with the Intel compiler. Process-core affinity was enforced using the `I_MPI_PIN_PROCESSOR_LIST` environment variable. The clock frequency was always fixed to the base value of the respective CPUs. Working sets were chosen large enough to not fit into any cache, i.e., at least ten times the last-level cache size on both systems. All floating-point computations were done in double precision. All experiments were performed for 500 k iterations (compute-communicate cycles), except for LBM where we used 100 k iterations. Each experiment was repeated at least five times to ensure that the runtime analysis is stable.

⁴ <https://hpc.fau.de/systems-services/systems-documentation-instructions/clusters/meggie-cluster/>

⁵ <https://hpc.fau.de/systems-services/systems-documentation-instructions/clusters/fritz-cluster/>

2.2 Synthetic microbenchmarks

We ran pure-MPI versions of the McCalpin STREAM Triad [10] ($A(\cdot)=B(\cdot)+s*C(\cdot)$) and a “slow” Schönauer vector Triad ($A(\cdot)=B(\cdot)+\cos(C(\cdot))/D(\cdot)$)⁶ with bidirectional next-neighbor communication. The saturation characteristics of these streaming kernels on one socket (ccNUMA domain) of Meggie are shown in Fig. 1. Each MPI rank i sends and receives messages to and from each of its direct neighbors $i + 1$ and $i - 1$ after each full loop traversal. Each array had 400 M elements, which yields a 9.6 GB working set for the STREAM Triad and a 12.8 GB working set for the Schönauer Triad. To mimic scalable applications, we set up a PISOLVER code which calculates the value of π by evaluating $\int_0^1 4/(1+x^2) dx$ using the mid-point rule with 500 M steps. Overall, four microbenchmark variants were employed:

1. MPI-parallel STREAM Triad with 5 MB messages
2. MPI-parallel STREAM Triad with 8 B messages
3. MPI-parallel “slow” Schönauer Triad with 8 B messages
4. MPI-parallel PISOLVER with 8 B messages

These four cases were run in two scenarios on the Meggie system: (A) open-chain process topology with 40 MPI processes on four ccNUMA domains (sockets), and (B) closed-ring process topology with 400 MPI processes on 40 sockets. Later these scenarios will be denoted “*Bench iA*” and “*Bench iB*”, respectively, where i is the label in the enumeration list above.

2.3 Proxy memory-bound parallel applications

We experiment with the following two MPI-parallel proxy applications and run them with 1440 MPI processes on 40 sockets of the Fritz system.

MPI-parallel LBM solver This is a prototype application based on a Lattice Boltzmann Method (LBM) from computational fluid dynamics using the Bhatnagar–Gross–Krook collision operator [5] and implementing a 3D lid-driven cavity scenario. It is purely memory bound on a single ccNUMA domain, but the halo exchange makes it communication dominated in strong scaling scenarios. The double-precision implementation employs a three-dimensional D3Q19 space discretization [11]. The domain decomposition is performed by cutting slices in the z direction. For halo exchange, five PDFs per boundary cell must be communicated. The MPI communication is done with non-blocking point-to-point calls, but no explicit overlapping of communication with useful work is implemented. We use an overall problem size of $n_x \times n_y \times n_z = 1440^3$ lattice cells, which amounts to a working set of 908 GB plus halo layers. Due to the one-dimensional domain decomposition, the communication volume per halo depends on n_x and n_y only and is independent of the number of processes.

MPI-parallel spMVM solver The sparse matrix-vector multiplication (SpMVM) $\vec{b} = A\vec{x}$ is a most relevant, time-consuming building block of numerous applications in science and engineering. Here, A is an $n \times n$ sparse matrix, and \vec{b} , \vec{x} are n -dimensional vectors. SpMVM plays a central role in the iterative solution of sparse linear systems, eigenvalue problems and Krylov subspace solvers. Due to its low computational intensity, the SpMVM kernel is mostly limited by the main memory

⁶ The low-throughput cosine and floating-point division shifts the bandwidth saturation point to a higher number of cores

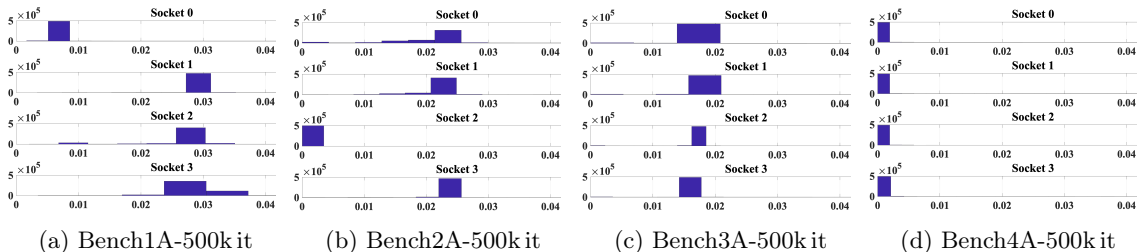


Fig. 3: Histograms sorting MPI times [sec] into bins for all benchmarks on the first process of each Meggie socket used in the run. The x -axes show the MPI times and the y -axes indicate the number of MPI time values in each bin.

bandwidth if the matrix does not fit into a cache. Our implementation uses non-blocking point-to-point communication calls, where the communication requests for reading the remote parts of \vec{x} are issued and then collectively finished via `MPI_Waitall`. After that, the whole SpMVM kernel is executed. The communication volume is crucially dependent on the structure of the matrix; the distribution of the nonzero entries plays a decisive role. In this paper, we use a matrix that arises from strongly correlated electron-phonon systems in solid state physics. It describes a Holstein-Hubbard model [6] comprising 3 electrons on 8 lattice sites coupled to 10 phonons. The sparse matrix A has 60,988,928 rows and columns and 889,816,368 non-zero entries, respectively, which leads to an average of 13 nonzeros per row and an overall data set size of 10.9 GB using four-byte indices in the Compressed Row Storage format (one-dimensional arrays for values, column indices, and row pointers).

2.4 Observables for analysis

We instrument all codes to collect the time stamps of entering and leaving MPI calls (MPI waiting time per process) at each iteration of each MPI process across the full run. From this data we construct a non-square matrix of size $N_p \times N_{it}$, where N_p is the number of MPI processes and N_{it} is the number of iterations. Each row (column) of the observable matrix represents the observable value, i.e., the time spent in MPI, for each process (iteration). There is a choice as to how this data can be used in analysis: One can either use the full timeline per process, which takes the end-to-end evolution of execution characteristics (such as desynchronization) into account, or cut out a number of consecutive iterations from different execution phases, which allows to investigate the development of interesting patterns in more detail. In addition, for some experiments we collect performance per MPI process averaged over the 1000 time steps.

3 Simple timeline metrics for analysis

3.1 Rank/ccNUMA-wise timelines and histogram of MPI time and performance

The histograms in Figure 3 sort the MPI time values of end-to-end (500 k iterations) runs of Bench[1–4]A into 35 bins. For memory-bound code, idle times are lower for desynchronized processes if the bandwidth saturation on a ccNUMA domain is weaker [2] (see Figure 3(c)). In the compute-bound PISOLVER case (Figure 3(d)), all processes are synchronized because of the absence of

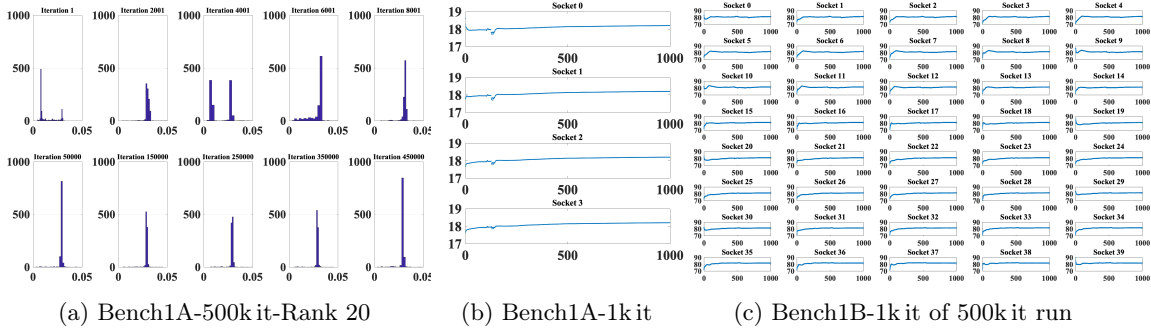


Fig. 4: (a) Snippet view of histograms for MPI times [sec] (x-axes) of rank 20 only and (b-c) performance [iterations/sec] (y-axes) on every first MPI process of each Meggie socket for the initial-zoomed 1 k iterations (x-axes) snapshot of Bench1A and Bench1B. Since the performance remains constant afterwards, we don't show the whole run of 500 k iterations.

any contention on the memory interface or on the network. Open-chain boundary conditions and strong memory contention ((a) and (b)) lead to a single synchronized socket. In the other cases, all sockets desynchronize gradually over 500 k iterations, which causes a spread in the histogram because processes evolve from lower to higher idle times. We have observed that this spread is more prominent for codes with stronger saturation and higher communication (*Bench1B*, LBM, and spMVM; data not shown for brevity).

We first investigate the open chain high communication overhead benchmark mode (*Bench1A*). Figure 4(a) shows the histograms at the different stages of evolution of a single MPI process (i.e., rank 20 on third ccNUMA domain) through the whole execution. Each histogram encompasses 1000 iterations. Initially (e.g., till 50 k iterations), the distributions are multimodal, which indicates different phases. On closer inspection it can be observed that the peak snaps from left to right as the process goes out of sync with its neighbors. This corroborates that the MPI waiting time is a good observable in our context. Since desynchronization cannot yield significant speedup if communication is insignificant, we show plots of performance vs. time step for significant communication cases only (*Bench1A* in Figure 4(b) and *Bench1B* in Figure 4(c)). These plots show the initial 1 k iterations. With open boundary conditions (b), one observes fluctuating performance as processes get desynchronized on all but one socket. However, this slow synchronized socket does not permit a global performance increase as desynchronized processes on other sockets cannot lag behind indefinitely. With closed boundary conditions (c), as the simulation progresses, performance (along with MPI waiting times) increases by about 15% and stays constant at the higher level till the end of the run.

3.2 Timeline in compact representation

MPI waiting times facilitate a compact representation of the timeline of a parallel program. Figure 5 show ranks on the x -axis and time steps on the y -axis, with the normalized MPI waiting time for each rank and time step color coded. For this representation, the mean value of MPI times across all processes and time steps is shown in white while red (positive value) and blue (negative value) represent values above and below the mean, respectively. This makes it possible to distinguish

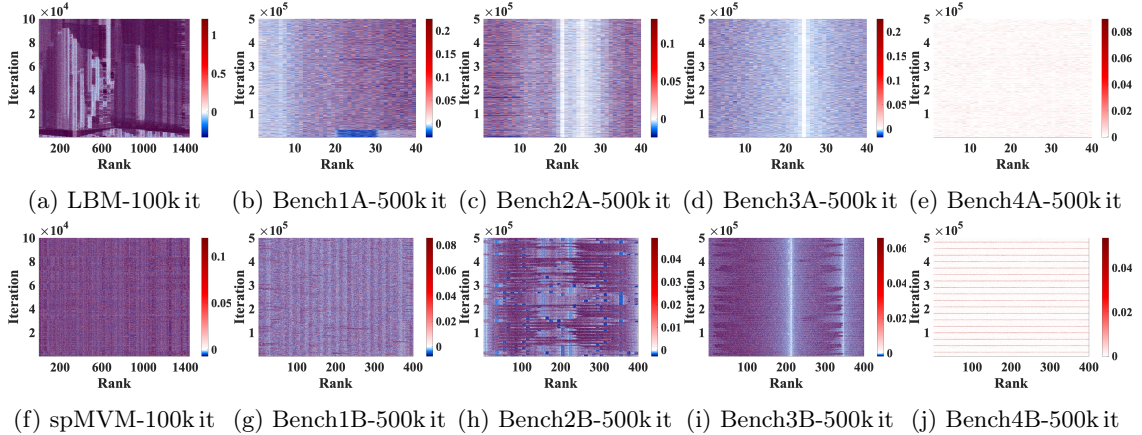


Fig. 5: Compact rank(x -axis)-iteration(y -axis) timelines of MPI waiting times [sec] for all benchmarks and full end-to-end runs.

between synchronized and desynchronized groups of processes: Strongly desynchronized processes spend more time in MPI (red), while white color marks synchronized processes (Ranks 1-10 and 20-30 in Figure 5(b) and (c), respectively). This visualization is similar to what tracing tools like ITAC or Vampir display; however, these tools often encompass too much information, and depending on the chosen resolution one can easily get lost in the data. In contrast, compact timelines of the waiting time per time step deliver a condensed view on this information and help to better visualize certain phenomena. For instance, the weaker saturation cases collect lower idle times which can be seen when comparing Figures 5(c)–(e) and (h)–(j). Asymptotic behavior in longer runs can be observed at the top part of the plot in all cases. Idle waves are prominently visible as dark-blue stripes in the LBM benchmark (Figure 5(a)).

4 Advanced metrics for analysis

Beyond timeline visualization and statistics, a plethora of advanced data analysis methods exist which can lead to deeper insights into the desynchronization process. Here we pick the *correlation coefficient* and the *phase space plot*.

4.1 Correlation coefficient

The correlation coefficient function [13] provides a simple way to uncover correlations between the timelines of two MPI processes. Figure 6 shows the color-coded correlation coefficients of rank pairs for all benchmarks, using the full end-to-end timelines. The matrices are obviously symmetric, and the diagonal entries (dark red) are set to one by convention. The correlation coefficients range from -1 to 1 , with -1 representing a direct, negative correlation, 0 representing no correlation, and 1 representing a direct, positive correlation. For the memory-bound applications, the ccNUMA domain structure is clearly visible in Figures 6(a-c,f-h). This implies that processes within ccNUMA domains are strongly correlated, while they are less (or not) correlated across sockets. The data

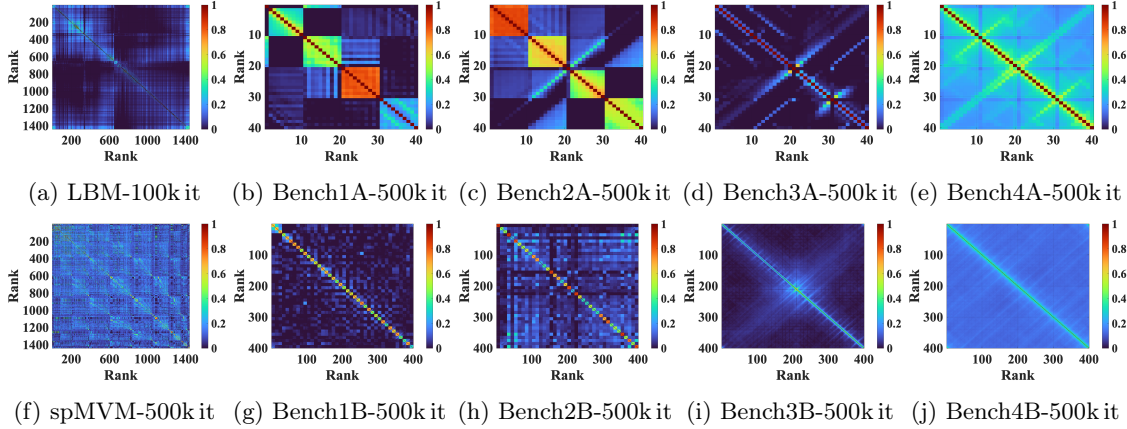


Fig. 6: Correlation coefficients of MPI times [sec] between process pairs for all benchmarks.

shows strong correlations within desynchronized sockets with a bi-modal distribution of MPI times since the socket already started to lose the sync pattern. In the open chain scenarios, processes on the last socket show a weaker correlation. In the SpMVM application, the sparse matrix structure is reflected in the correlation coefficients since the desynchronization process is strongly influenced by the communication structure (Figure 6(f)). In weakly or non-saturated applications (Figures 6(d-e, i-j)), correlations are generally weaker, as expected.

4.2 Phase space plots

In order to capture the temporal evolution of MPI waiting time, we set up a scatter plot where each data point has coordinates $(\text{MPItime}(t_i, r), \text{MPItime}(t_i + 1, r))$. For each process, a fixed point in this “phase space” is a point on the slope-1 line through the origin. If the waiting time evolves, a process will move through the first quadrant; if waiting time increases over time (e.g., due to desynchronization), the path of a process will rise above the axis and move further up and to the right. Color coding in the point cloud, from early (blue) to late (yellow), helps to visualize how processes move. We choose two different types of analysis.

In the *snippet view*, only a small part (e.g., 1000 iterations) of the data is visualized per plot; separate plots are used to show the long-term temporal evolution (*initial-mid-end* in Figure 7). In Figures 7(a)–(c), after the initial in-sync phase, the cloud gets spread out. Asymptotically, we identify multiple weak and strong clusters (smaller and bigger attractors basin for observable). Stronger or weaker clustering along the diagonal line expresses how much the observable fluctuates around a “steady-state” value. In the example shown, all but one (blue points) sockets get desynchronized. This separation of sockets should go away as time progresses for the close chain scenario (see Figures 7(f)–(h)), but obviously the progression is too slow to be discernible in this visualization. For PISOLVER (Figures 7(d)–(e)), the point cloud starts around the origin and remains there since this scalable code is self-synchronizing.

In the *overall view* (see Figure 8), the full timeline is shown for one process in one plot (plotting all processes would not allow useful conclusions). Here the gradual evolution of waiting time is hard to see since it is drowned in fluctuations. However, especially in the open-chain scenarios

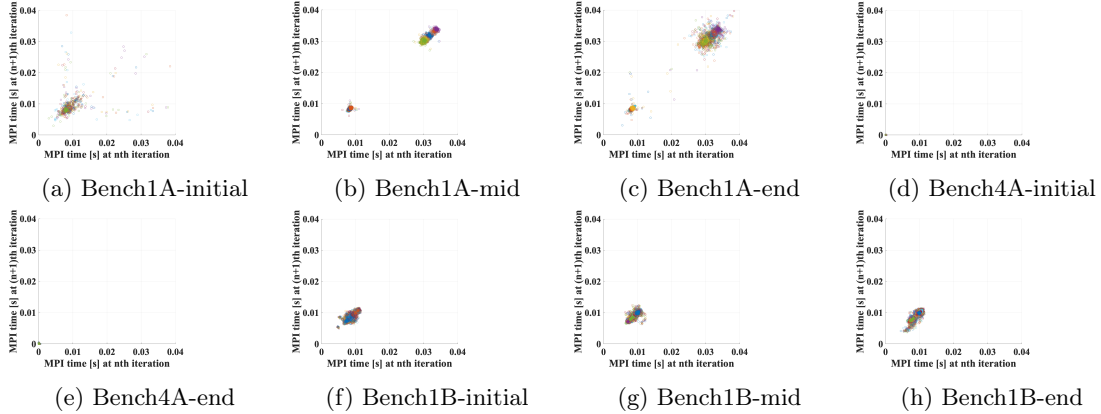


Fig. 7: (a, c, f, h) *Snippets view* of phase space of all MPI processes for 100 iterations at the beginning. (b) Snapshot of 1 k iterations (9.9-10 k iterations) for LBM in the middle state. (d, e, g, i, j) Snapshot of 1 k iterations in the middle (1.9-2 k iterations) and at the end evolved state (499.9-500 k iterations).

(Figures 8(b)–(d)) we observe structures parallel to the axes, indicating singular long delays of a few preferred lengths. These are signatures of traveling idle waves, which for a single process manifest themselves as singular high waiting time in one time step.

5 Machine learning techniques for analysis

In order to prepare the timeline data for machine learning techniques, we subtract the mean values of MPI times across all time steps and processes of each experiment from the value at each step. This is one of many possible options for data normalization; better ones might exist. We then apply PCA [7] to the timelines of each run, using the MPI times of each process as feature vectors, and then classify the projections of the feature vectors on the first two principal component vectors using clustering techniques. Finally, we validate the quality of the clustering for an accurate evaluation. To do that, we look at the reconstruction error that is generated using an essential number of Principal Components only.

5.1 Principal Component Analysis (PCA)

Principal Component analysis projects the directions of high-dimensional data onto a lower-dimensional subspace while retaining most of the information. Ideally, the low-dimensional manifolds still retain almost all variance of the data set needed to identify and interpret generic behavior. Coarse features are captured by the first principal components while the highest-frequency features are captured by highest principal components. PCA centers the data and uses the *singular value decomposition* algorithm on the non-square observable matrix. Rows and columns of the input matrix correspond to observations and variables, respectively. Each row vector is the timeline of MPI times in a process; the observable values in different iterations are the coordinates in a high-dimensional space.

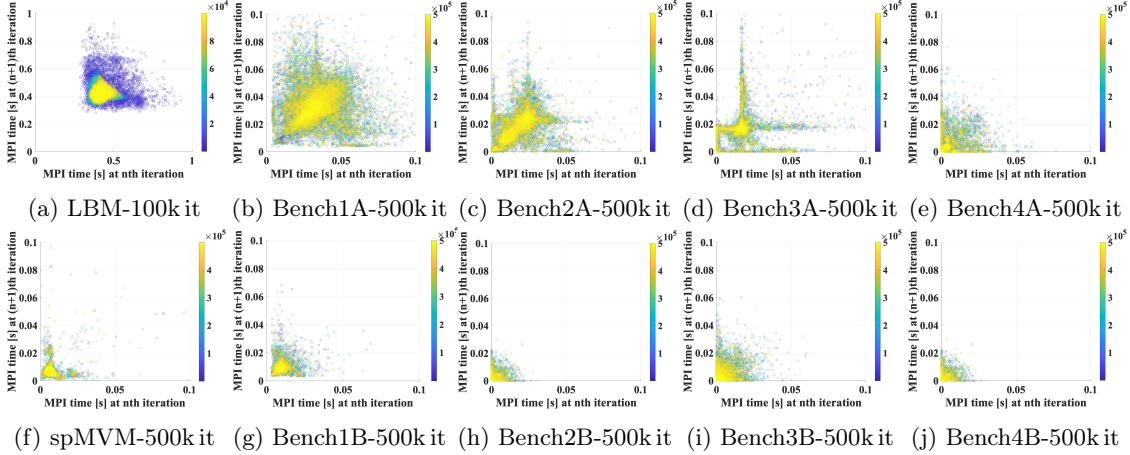


Fig. 8: *Overall view* of phase space for one MPI process (rank 32) of all benchmarks. The axes show the time spent in the MPI library at the n -th and $(n + 1)$ -th iteration, respectively.

Projection plot on the reduced Principal Components The points in Figure 9(a, e) indicate the score of each observation for the first three principal components in the Bench1B experiment. They show the PCA analysis on the full run and on the last 1000 iterations, respectively. For the compute-bound PISOLVER (Bench4), all processes cluster around one point because of absence of contention on the sockets (data not shown). In contrast, for the memory-bound Triad variants, four or 40 clusters emerge at the start due to the presence of four or 40 ccNUMA domains, respectively. As time progresses, all desynchronized sockets form weak clusters by collecting larger scores for PC1 and nonzero scores for PC2, while the in-sync domain forms a compact cluster due to lower scores for PC1 and zero scores for PC2. Desynchronization is strongest for the processes on the top right of the plot. The negative values for projections on eigenvectors indicate an inverse relationship, but large (either positive or negative) values indicate that a vector has a strong overlap with that principal component. If all ccNUMA domains are eventually desynchronized, all processes cluster on the top right as shown in Figure 9(e) for the last 1000 iterations.

Principal Components (eigenvectors) In order to get better insight into the governing characteristics of desynchronized execution, We analyze the essential eigenvectors. Figures 9(c, d) show the eigenvectors and how ranks contribute to the reduced number of principal components for the full run and the last 1000 iterations. In the full-run case (Fig. 9(c)), the PC1 eigenvector characterizes desynchronizing processes and thus indicates a lot of waiting times with in-between downward spikes. The PC2 eigenvector characterizes in-sync processes and shows almost no waiting time, but upward spikes (idle periods) in between. It must be noted that the PCs for end-to-end runs encompass the entire evolution of the program, including initial in-sync phases, transient states, and final, stable states. Looking at the final 1000 iterations (Fig. 9d), the signatures are much clearer; PC1 characterizes stable desynchronization while PC2 maps transient behavior where a noise-induced event between iteration 600 and 700 causes processes to change from a state with small waiting times to a state with large waiting times. One can interpret this as processes within a ccNUMA domain “snapping” out of sync.

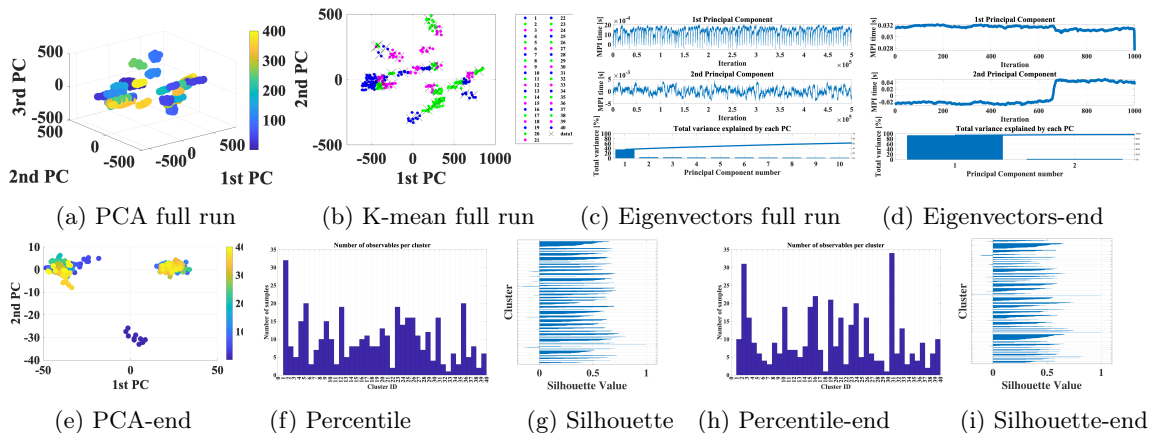


Fig. 9: Principal Component analysis, k-mean clustering, eigenvectors, percentile and Silhouette analyses of Bench1B (a-c, f-g) for the whole run time of 500k iterations and (d-e, h-i) for snapshot of last 1 k iterations only.

Total variance explained by each principal component The percentage of the total variance explained by each principal component (Pareto plots in Figures 9(c-bottom, d-bottom)) indicates for Bench1B how many PCs are required to reconstruct the original data sets using only the projections. In this particular case, one component is sufficient near the end of the run but many are required (with the first one still dominating) over the full run. Overall, the results show that more PCs are needed to explain the data variance for a more pronounced memory-bandwidth saturation on the ccNUMA domain. In contrast, the compute-bound PISOLVER has much less variance as no typical structure exists except natural, noise-induced fluctuations. Further, the more revealing socket behavior in short-runs is captured by the higher number of PCs compared to the asymptotic behavior in long runs.

5.2 K-means clustering

While PCA delivers insight into typical patterns, it does not allow for automatic grouping (clustering) of processes. This can be accomplished by partitioning the projection of observations on the principal components into k clusters by using k-means. Rows of PC scores correspond to points and columns correspond to variables. We use the k-means++ algorithm [12] for the cluster center initialization; it is strongly dependent on the distance metric used.

Distance types Clustering quality was studied for four metrics. In the cluster, each centroid c is either the mean $((x-c)(x-c)')$ or component-wise median $((\sum_{j=1}^p |x_j - c_j|))$ of the points in *squared Euclidean* and *city-block* metrics, respectively. Here, x is a row of PC scores. For the *cosine* and *correlation* metrics, each centroid c is either the mean of the points which are already normalized to unit Euclidean length $(1 - \frac{xc'}{\sqrt{(xx')(cc')}})$ or component-wise mean of the points which are already centered

and normalized to zero mean and unit standard deviation $(1 - \frac{(x - \bar{x})(c - \bar{c})'}{\sqrt{(x - \bar{x})(x - \bar{x})' \sqrt{(c - \bar{c})(c - \bar{c})'}}})$,
with $\bar{x} = \frac{1}{p}(\sum_{j=1}^p x_j)1_p$ and $\bar{c} = \frac{1}{p}(\sum_{j=1}^p c_j)1_p$.

The result is a matrix containing the k cluster centroid locations and a vector containing cluster indices. Figure 9(b) shows a scatter plot of essential PC scores grouped by the cluster indices of each observation in the *Bench1B* case. K-means uses the squared Euclidean distance here. We expect one cluster if all processes are in a fully evolved desynchronized state.

Number of observables per cluster The number of clusters k is chosen in a way that it assigns all unlike clusters, while the number of observables belonging to each cluster could be significantly different. Figures 9(f, h) show the histogram bar chart of the cluster indices in the vector, which are sorted into k bins. We choose k equal to the number of ccNUMA domains. The x -axis indicates the cluster IDs and the y -axis shows the number of samples.

Validation of clustering quality A potential application of Principal Component analysis is its evaluation by calculating the error between original and reconstructed signal from fewer PCs. To this end, one can reconstruct the signal by multiplying the scores with the first two PCs and then sum them up. This should be very close to the original signal if the reconstruction error (using the Euclidean norm) is less than some threshold value. In Figures 9(g, i), we performed a Silhouette analysis [8] to quantify the quality of the clustering. A highly representative clustering is associated with a large positive coefficient value close to one and indicates that the point is well matched to other points in its own cluster, and poorly matched to other clusters. On the other hand, a negative coefficient value represents a disqualified clustering. We get higher reconstruction error for the high-frequency signal of the PISOLVER case as expected. While exploring the influence of distance metrics, it turned out that *cosine* is the best-suited and *city-block* is the worst-suited distance metric.

6 Summary and future work

Key takeaways We have presented expressive data analytics techniques for investigating the dynamics of MPI-parallel programs with regular compute-communicate cycles. We consider MPI waiting time per time step and process as a good observable metric since it encompasses much of the relevant dynamics in a very condensed format. Our new “phase space” analysis based on this data provides an efficient, visual way to observe the evolution of a program from its initial, synchronized state into a desynchronized state. However, it is not strictly a data analytics technique since it involves manual inspection of the data (moving dot clouds). PCA and subsequent k-means clustering allow for a more automated analysis, providing feature extraction, i.e., typical timeline behavior, as well as grouping of MPI processes into clusters with similar features. Hence, these methods could pave the way towards advanced job-specific monitoring of production jobs on clusters. We have also found that the analysis is more expressive when applied to snippets of the timeline in order to avoid mixing different characteristics. If one is interested in an evolved state only, the final iterations of a run are most relevant.

Future work We are convinced that PCA applied to MPI waiting time data allows the investigation of unknown applications by mapping their temporal evolution to principal components found in

prototypical benchmark runs. It is still an open question how to choose these benchmarks to extract relevant, distinguishable patterns that real application can be tested against. It will also be necessary to investigate how the waiting time metric should be normalized to be as generic as possible. Furthermore, we plan to apply the demonstrated techniques to a wider spectrum of real applications in order to fathom their true scope of applicability.

Acknowledgments

This research work is supported by KONWIHR, the Bavarian Competence Network for Scientific High Performance Computing in Bavaria, under project name “OMI4papps.” We are thankful to Dr. Thomas Zeiser and his admin team for excellent technical support on NHR@FAU systems.

References

- [1] A. Afzal et al. Analytic modeling of idle waves in parallel programs: communication, cluster topology, and noise impact. In B. L. Chamberlain et al., editors, *Lecture Notes in Computer Science* (Virtual, Online), volume 12728 LNCS, pages 351–371. Springer Science and Business Media Deutschland GmbH, June 24–July 2, 2021. DOI: 10.1007/978-3-030-78713-4_19.
- [2] A. Afzal et al. Desynchronization and wave pattern formation in MPI-parallel and hybrid memory-bound programs. In P. Sadayappan et al., editors, *Lecture Notes in Computer Science* (Frankfurt), volume 12151 LNCS, pages 391–411, Cham. Springer International Publishing, June 22–25, 2020. DOI: 10.1007/978-3-030-50743-5_20.
- [3] A. Afzal et al. Propagation and decay of injected one-off delays on clusters: A case study. In *2019 IEEE International Conference on Cluster Computing, CLUSTER 2019, Albuquerque, NM, USA, September 23-26, 2019*, pages 1–10, 2019. DOI: 10.1109/CLUSTER.2019.8890995.
- [4] A. Afzal et al. The role of idle waves, desynchronization, and bottleneck evasion in the performance of parallel programs, 2022. arXiv: 2205.04190 [cs.DC].
- [5] P. L. Bhatnagar et al. A model for collision processes in gases. I. Small amplitude processes in charged and neutral one-component systems. *Physical review*, 94(3):511, 1954.
- [6] H. Fehske et al. Quantum lattice dynamical effects on single-particle excitations in one-dimensional Mott and Peierls insulators. *Physical Review B*, 69(16):165115, 2004.
- [7] I. T. Jolliffe et al. Principal component analysis: a review and recent developments. *Philosophical Transactions of the Royal Society A: Mathematical, Physical and Engineering Sciences*, 374(2065):20150202, 2016.
- [8] L. Kaufman et al. *Finding groups in data: an introduction to cluster analysis*. John Wiley & Sons, 2009.
- [9] S. Markidis et al. Idle waves in high-performance computing. *Physical Review E*, 91(1):013306, 2015. DOI: 10.1103/PhysRevE.91.013306.
- [10] J. D. McCalpin et al. Memory bandwidth and machine balance in current high performance computers. *IEEE computer society technical committee on computer architecture (TCCA) newsletter*, 2(19–25), 1995.
- [11] Y.-H. Qian et al. Lattice BGK models for Navier-Stokes equation. *EPL (Europhysics Letters)*, 17(6):479, 1992.
- [12] S. Vassilvitskii et al. K-means++: the advantages of careful seeding. In *Proceedings of the eighteenth annual ACM-SIAM symposium on Discrete algorithms*, pages 1027–1035, 2006.
- [13] W. T. Vetterling et al. *Numerical Recipes: Example book C*. Cambridge University Press, 1992.